Progress in Physics of Applied Materials 2 (2022) 139–146

Semnan University

Progress in Physics of Applied Materials

journal homepage: https://ppam.semnan.ac.ir/

# Oxygen and nitrogen doped diamond-like carbon thin films: A comparative study

**R. Zarei Moghadam[1*], M. Taherkhani[2]**

[1]*Department of Physics, Faculty of Science, Arak University,38156-8 8349 Arak, Iran*
[2]*Faculty of Physics, Semnan University, P.O. Box: 35195-363, Semnan, Iran*

**ARTICLE INFO**

Article history:
Received: 20 November 2022
Revised: 5 December 2022
Accepted: 17 December 2022

Keywords:
Si substrates
Direct ion beam
DLC films
Raman spectroscopy
water contact angle

**ABSTRACT**

DLC films were deposited on Si substrates using direct ion beam deposition method, followed by investigating the influence of $O_2$ and $N_2$ doping on their electrical and structural properties. The films were doped with oxygen and nitrogen under flow rates of 5 and 40 sccm (standard cubic centimeters per minute). The structure of the films was studied by Raman spectroscopy. Result showed that by increasing oxygen incorporation, $sp^2$ content decreases, $sp^3$ content increases, and the C-C bonding loses its order. As the size of the $sp^2$-rich cluster increased with $N_2$ content, the disorder in the DLC samples decreased, leading to a decrease in the FWHM of the G peak. The water contact angle measurement showed that an increase in oxygen flow ratio results in a decrease in contact angle from 82.9° ± 2.1° to 50° ± 3°. With increasing nitrogen flow rate from 5 to 40, the contact angle of DLC thin films increased from 78° to 110°.

## 1. Introduction

Diamond-like carbon (DLC) has been the subject of intensive study for over 40 years [1]. DLC films have attracted the attention of many studies due to the combined properties of graphite and diamond, such as high water repellency and hardness, wear resistance, and good optical coefficient, among other features [1-5]. DLC film has unique properties such as large Young's modulus, high hardness, low coefficient of friction, high hydrophobicity, and chemical inertness [1]. DLC films have been used as protective storage devices, solar cell coatings, and wear reduction [2, 3]. There are various methods for the deposition of DLC films, such as pulsed laser deposition (PLD) [4], direct ion beam [1], plasma enhanced chemical vapor deposition (PECVD) [5], DC, and magnetron sputtering [6]. To improve properties such as stress, optical, mechanical, etc., many authors have studied the doping effects of DLC films with various elements such as O, Si, B, N, and Ag [7-11]. It has been reported that by incorporating nitrogen into DLC coatings, friction and internal layer stress can be reduced [12]. In DLC thin films, the mechanical properties, such as residual stress, mainly depend on the amount of $sp^3$ bonding, which is mainly affected by the ion energy, and is equal to the growth and doping parameters [13, 14]. The residual stress in DLC thin films can be reduced through doping by various elements. Oxygen has been considered as an optical impurity element that has the ability to modify the surface properties of DLC films. [10]. An efficient polarization effect is predicted because of the high electronegativity of oxygen.

Among various elements, nitrogen has been widely studied for use as a dopant in DLC thin films, which helps to reduce the stress of DLC thin films [15]. When nitrogen is incorporated into a thin layer of DLC, C-N groups are formed and act as electron acceptors due to their strong electron withdrawing ability [16]. Kopustinskas et al. prepared α-CNx:H layers by direct ion beam from $C_6H_{14}$ + $H_2$ + $N_2$ gas mixture on Si (100) substrate and observed that the refractive index, growth rate, and sp3 bonding decreased due to the increase of nitrogen in the gas mixture. found and mixture and found more graphite-like formation was present [17]. Tsuchiya et al reported the preparation of DLC films doped with nitrogen by PECVD technique by $CH_4$, $N_2$ and Ar gases on Si substrate and also investigated the effect of $N_2$ composition on their structural, electrical, optical, and mechanical properties [18]. They described that the internal stress of the as-prepared DLC samples (less than 0.5 GPa) reduced to less than 13.6% by N doping at $N_2$ flow and the electrical resistivity (less than $10^{-2}$ Ω.cm) was reduced [18]. Hwang and his colleagues studied the effect of oxygen and

* Corresponding author. Tel.: +98-9140104665
*E-mail address: r.zarei1991@gmail.com*

DOI: https://doi.org/10.22075/ppam.2022.29057.1043

nitrogen contamination on the optical properties of diamond-like carbon layers [11]. The aim of this article is to achieve hydrophilic and hydrophobic thin layers by using oxygen and nitrogen gases. The main purpose of this work is to comprehensively compare the structural, electrical, and wettability properties of diamond-like carbon thin films. In the works of others, the comparison of oxygen and nitrogen gas doped has not been clearly studied.

In the present study, O-DLC and N-DLC films were deposited on Si substrates by direct ion beam at room temperature. This study reports the effect of $O_2$ doped and $N_2$ doped on the electrical resistance, hydrophobicity, and structural properties of the prepared DLC films. Raman analysis was used to investigate the structural properties of O-DLC and N-DLC samples. The internal stress was measured by calculating the curvature of the layers after deposition and by using the Estonian equation. Electrical resistivity (ρ) of O-DLC and N-DLC samples was measured using a four-point probe instrument.

## 2. Experimental Details

### *2.1. Deposition method*

In recent years, researchers have been interested in the development of deposition using increased particle flux for various applications such as space ion thrusters and plasma accelerators. Figure 1 shows a cross-sectional view of the source of the anode layer. As shown in this figure, the anode layer source consists of SmCo permanent magnet, gas inlet, inner and outer cathodes, magnet poles and anode with water channel cooling. The anode layer system was powered by DC power supply in voltage regulation mode. As an advantage, there is no electron source using this method, so gases such as oxygen, nitrogen or other reactive gases can be used. The gas is directly injected into a discharge channel. The suspension of electrons and the maintenance of a strong electric field in the discharge plasma both result from a strong magnetic field between the inner and outer poles.

### *2.2. Deposition process*

N-DLC and O-DLC samples were prepared using an anode layer system by 150 sccm CH4 (high purity > 99.999%) on glass and Si (100) substrates with a thickness of 2.05 mm and a diameter of 34.91 mm. These films were kept at room temperature. Si (100) substrates were cleaned in an ultrasonic bath with acetone and, then, dried by high purity N2 gas (purity 99.999%). Substrates were fixed on a stationary holder approximately 15 cm away from the ion source. DLC thin films were doped with oxygen flow rates (5 and 40 sccm) and nitrogen flow rates (5 and 40 sccm). The samples were named as $O_5$-DLC, $O_{40}$-DLC, $N_5$-DLC and $N_{40}$-DLC. For methane deposition, a discharge voltage of 1 kV was applied between the cathode and anode of the ion gun. For all processes, the pressure in the vacuum system was $6\times10^{-6}$ mbar and the pressure during the deposition process was $3\times10^{-3}$ mbar.

The structural properties of the DLC samples were also investigated by Raman analysis (Tacram P50C0R10 model, excitation wavelength 532 nm). The internal stress was calculated according to the Stoney equation from the radius of curvature of the layers measured by the optical interferometry. The hydrophobic properties of DLC thin films were measured by a tilting plate stand, CCD-video microscope and prism, and the images were analyzed using Digimizer software.

## 3. Results and discussion

### *3.1. Raman characterization*

Raman spectroscopy technique was used to analyze the structural properties of DLC films. Raman analysis is a standard, non-destructive tool for characterizing DLC bond nature and microstructural information [19]. Raman peaks of DLC films were fitted by two Gaussian line shapes. The broad Raman peak of DLC films is usually an overlap of two peaks: 1. D (disorder) peak around wavenumber of 1370 $cm^{-1}$ and 2. G (graphite) peak around wavenumber of 1500-1650 $cm^{-1}$. D peak is a breathing mode of symmetry phonons arising from $sp^2$ carbon atoms in the ring. This mode is only activated in disorder and its peak intensity is strongly related to the presence of a sixfold aromatic ring [20]. The G peak originates from the stretching vibration of each $sp^2$ site pair in both the ring and the chain [21]. From the fitting of the Raman spectra, the position of the G peak, the ratio of the intensity of the D peak to the G peak ($I_D/I_G$), and the full width at half maximum (FWHM) of the G peak can be extracted. Figure 2 shows the fit of the two Gaussian peaks of the $O_5$-DLC and $O_{40}$-DLC samples. Basically, we can see the movement of peak G to higher values and the increase of intensity of peak D with the increase of $O_2$ gas flow rate in the figure. The FWHM values of G peak of $O_5$-DLC and $O_{40}$-DLC samples were estimated to be 192 and 114 $cm^{-1}$, respectively. The FWHM of D peak values of $O_5$-DLC and $O_{40}$-DLC samples were estimated to be 186 and 120 $cm^{-1}$, respectively. The values of G peak position of $O_5$-DLC and $O_{40}$-DLC samples were estimated to be 1530 and 1586 $cm^{-1}$, respectively. The values of D peak position of $O_5$-DLC and $O_{40}$-DLC samples were estimated to be 1298 and 1376 $cm^{-1}$, respectively. The values of the ID/IG ratio of $O_5$-DLC and $O_{40}$-DLC samples were estimated to be 0.55 and 1.17, respectively. If the oxygen concentration is higher, for example, $O_{40}$-DLC samples, the $I_D/I_G$ ratio and G peak position increase again and the FWHM (G) decreases, indicating $sp^2$ cluster ordering. FWHM is a measure of the bond length disorder, and the ID/IG ratio is the size of the $sp^2$ phase organized in the rings. A decrease in ID/IG ratio means an increase in $sp^3$ content. A large FWHM value indicates disorder due to a larger bond angle and length [22]. FWHM and G peak position of O-DLC samples versus $O_2$ gas flow rate are shown in Figure 3. These results show that with an increase in oxygen incorporation, the $sp^2$ content decreases while C-C and $sp^3$ bond disorders increase the content [23]. In this regard, the increase in the G peak position and the $I_D/I_G$ ratio indicates the order of the $sp^2$ clusters [24]. The chain-like sites have more C-H bonds compared to the aromatic sites. Hence, as the $O_2$ content of DLC films increases, the hydrogen content of

the films decreases. Dwivede et al. [25] reported that the ID/IG ratio, G peak position, and $sp^2$ clustering decreased with increasing plasma $O_2$ in DLC films. McKindra et al

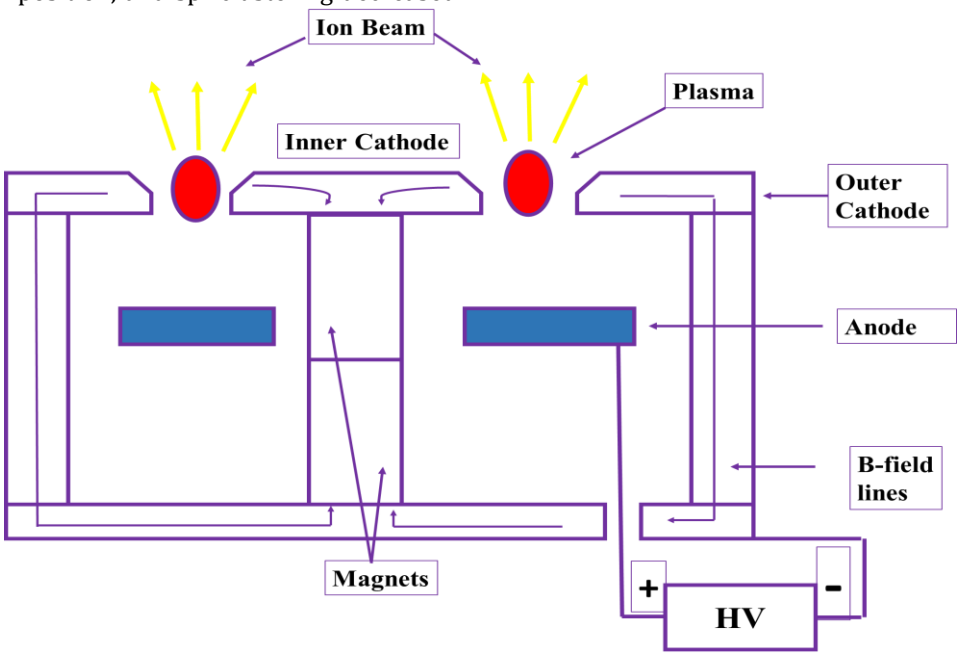


**Fig. 1.** Schematic of the source of the anode layer and the working principle.

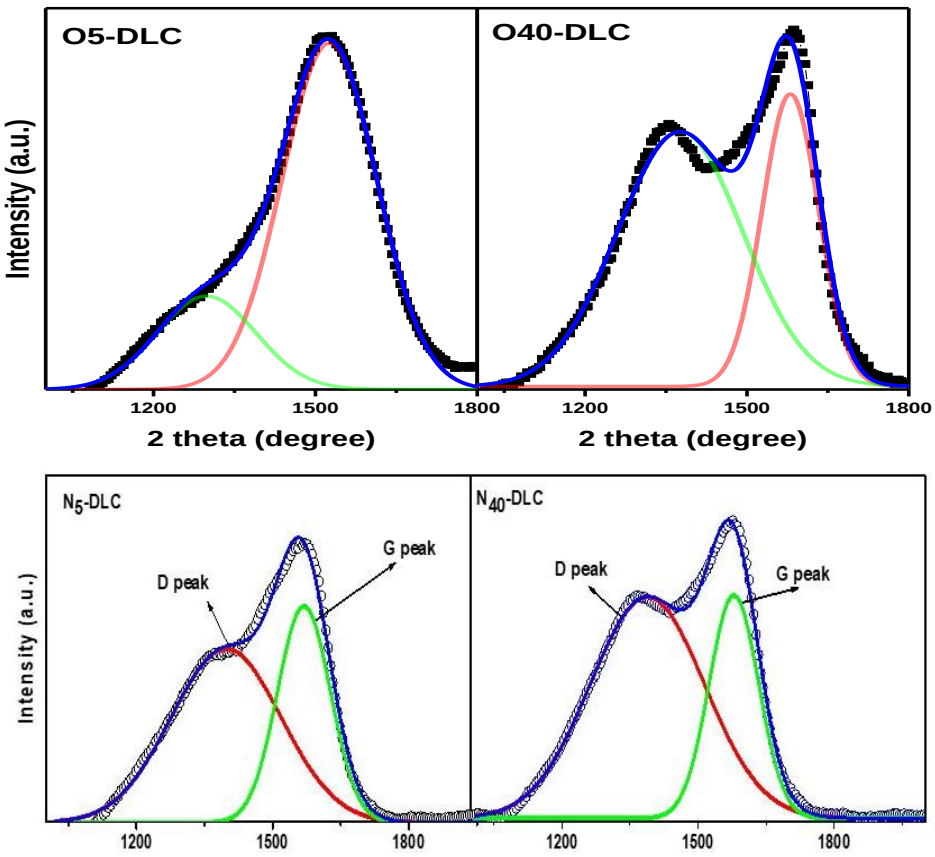


**Fig. 2.** Fitted two Gaussian peaks for the $O_5$-DLC, $O_{40}$-DLC, $N_5$-DLC, and $N_{40}$-DLC samples.

[26] deposited $O_2$-doped films using magnetron sputtering and reported a decrease in $I_D/I_G$ ratio followed by an increase in $O_2$ content.

Fig. 2 shows the fitting of the two Gaussian peaks of the $N_5$-DLC and $N_{40}$-DLC thin films. Basically, it is possible to see the movement of peak G to higher values and the increase of intensity of peak D with increasing $N_2$ gas flow rate in the figure. The position of G peak and FWHM of

DLC samples versus $N_2$ gas flow rate are shown in Figure 3. It can be seen from the figure that with the increase of

$N_2$ content, the position of the G peak is shifted to higher wave numbers. DLC thin films were also observed to become graphitized, which could be due to the growth and formation of $sp^2$ clusters [27]. These behaviors were related to the structural arrangement of DLC samples [28]. Lee et al. [28] reported that the position of the G peak shifted to higher intensities with increasing $N_2$ content.

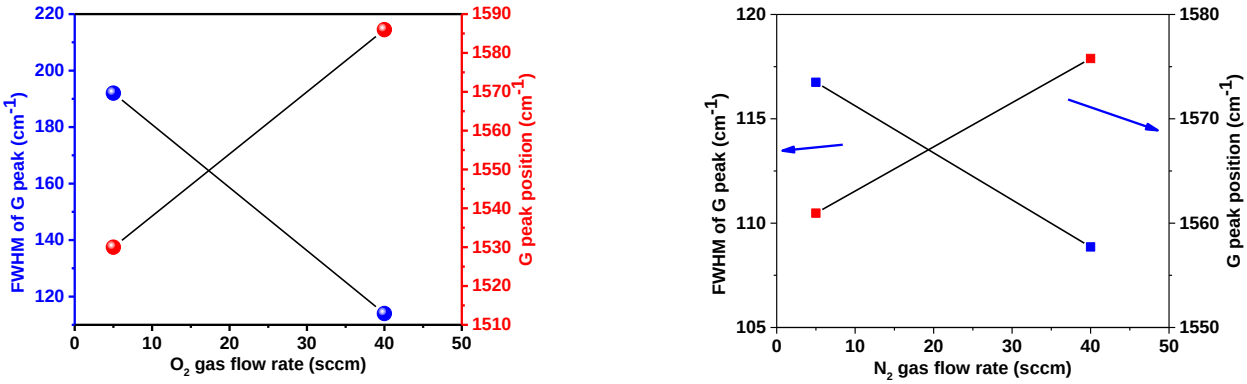


**Fig. 3.** FWHM and G peak position of the $O_5$-DLC, $O_{40}$-DLC, $N_5$-DLC, and $N_{40}$-DLC films.

Tsuchiya et al [18] prepared N-doped DLC films by PECVD technique and studied the effects of N content on the structural properties. They showed that the G peak shifted to higher wavenumbers with increasing $N_2$ content, which could be due to the structural order of the DLC films. As the $N_2$ content increased, the FWHM of the G peak shifted to a lower wavenumber. As the size of the $sp^2$-rich cluster increased with $N_2$ content, the disorder in the DLC samples decreased, leading to a decrease in the FWHM of the G peak [29]. Polaki et al. [29] reported that DLC samples were deposited on a Si (100) as a function of $N_2$ content by the PECVD technique. They showed the graphitic structure in the DLC samples with increasing $N_2$ flow rate.

### *3.2. Evaluation of internal stress*

To calculate the internal stress of all the samples, a glass slide (diameter 34.91 mm and thickness 2.05 mm) was chosen. The internal stress was measured by calculating the curvature of the film after deposition on one side through Stoney's relation [30]:

$$\sigma = \frac{E_S}{6(1-\nu_S)}\left(\frac{t_S^2}{t_f}\right)\left(\frac{1}{R_2}-\frac{1}{R_1}\right) \qquad (1)$$

Where σ is the internal stress, $\nu_s$ is the substrate Poisson's ratio, $E_s$ is the substrate, Young modulus, $R_1$ and $R_2$ are the substrate curvatures before and after deposition, $t_s$ and $t_f$ are the thicknesses of substrate and film, respectively. The adopted values for the glass substrate constants ($\nu_s$=0.22, $E_s$=1.03×10$^{10}$ Nm$^{-2}$) were taken from Zou et al. [31]. The internal stress of O-DLC and N-DLC samples was calculated by the stress induced from the interferometric surface profiler. The radius (R) of the substrates before and after the deposition was calculated using the observation of Newton's rings method by the optical interferometry. The radius of the substrate curvature was determined through the following equation [32]:

$$R = \frac{d_m^2}{4m\lambda} \qquad (m=1, 2, 3, \ldots) \qquad (2)$$

Where $d_m$ is the $m^{th}$ dark interference fringe diameter and $\lambda$ is the wavelength of the light ($\lambda$=589.3 nm).

As the oxygen flow rate increased from 0 to 40 sccm, the internal stress decreased from 2.7 to 0.11 GPa. The mechanical properties of DLC thin films depend on the $sp^2/sp^3$ fraction and H content in the film structure [33, 34]. DLC (a-C:H) films have been reported to contain both $sp^2$ and $sp^3$ sites, and the $sp^2$ sites segregate into clusters embedded in an $sp^3$ band matrix [35]. Increasing the hydrogen content in the DLC film structure breaks $sp^3$ C-C bonds, which are bonding clusters, and aromatic $sp^2$ C=C, which are inside the clusters. When $sp^3$ C-C bonds are broken and $sp^3$ C-H bonds are formed, a discontinuity is created in the network of the films, and then their residual stress decreases.

As the $N_2$ content increased from 5 to 40 sccm, the internal stress decreased from 1.63 to 0.58 GPa. Silva et al reported similar results for N-DLC thin films [36]. Three important factors were the reduction of internal stress, the increase of $sp^2$-C bonds [37], the distortion of the bond angle and the increase of induced ad-atom mobility [38]. Raman analysis confirmed that incorporation of $N_2$ into DLC films increased the amount of $sp^2$ hybridized atoms. In addition, the incorporation of $N_2$ reduced the coordination number of the films, which in turn reduced the degree of over-confinement in the N-DLC samples; therefore, it reduced the stress [39]. In addition, with the incorporation of $N_2$, C≡N bonds were formed, which resulted in a weak network between the internal stress of N-DLC samples [40].

### *3.3. Electrical resistivity*

In the present research, the electrical resistance (ρ) of O-DLC and N-DLC samples was measured using equation (3) [41] with the help of a four-point probe tool. For this purpose, Rs, which is calculated from the I-V characteristic curve, was taken into account.

$$\rho = \frac{\pi t}{\ln 2} R_s \quad (3)$$

Where t is the thickness of O-DLC and N-DLC films. Figure 4 shows the change in electrical resistance as a function of oxygen flow rate. As can be seen, increasing the oxygen flow rate causes a significant increase in the electrical resistance of O-DLC films. Electrical resistance depends on carrier density, cluster size, and mobility [42]. $I_D/I_G$ ratio and cluster size increase as the number of loops per cluster increases and the number of π states per cluster decreases. It may be inferred that the increase in electrical resistance is due to the decrease in the number of π states in each cluster [42]. Replace by Zarei Moghadam et al. [41] reported that the increase in electrical resistance could be related to the increase in the fraction of $sp^2$ bonds or the crystallization of DLC films. Some authors believe that the Formation of C-H bonds can significantly influence the electrical resistance of DLC films [43, 44]. DLC film resistance for $O_5$-DLC to $O_{40}$-DLC samples increased from $0.83\times10^2$ to $1\times10^5$ Ohm/cm. This can be explained by the fact that high-energy ion bombardment on the surface of the growing films is one of the main parameters that control the ad-atom mobility on the film surface and thus their structure. Therefore, the plasma self-bias changes with increasing oxygen flow rate, so that changing the oxygen flow rate can change the energy of the ions bombarding the film surface.

As shown in Fig. 4, the resistivity of the DLC films decreased significantly from $3.7 \times 10^4$ Ω·cm to $0.83 \times 10^3$ Ω·cm under a low nitrogen flow rate of 5 sccm, and a further increase in the nitrogen flow rate to 40 sccm led to a slight decrease of the film resistivity. Two main reasons for the decrease in resistivity have been suggested: (1) the increase in $sp^2$ content, i.e., graphitization by N doping in DLC films, led to a decrease in electrical resistivity. (2) As mentioned above, incorporated N reduces the band gap [45] and also acts as a good electron donor in DLC films to reduce resistance, which is also reported in the literature [46]. On the other hand, nitrogen can form essentially three possible aromatic compounds with carbon. The first is substitution into a six-membered ring, which results in three σ bonds to three carbon atoms.

### *3.4. Surface contact angle*

A microscope equipped with CCD-video was used to measure the surface contact angle of O-DLC and N-DLC samples, a tiltable plate stand and a prism. The images taken by this method were analyzed by Digimizer software. Figure 5 shows the dependence of oxygen flow rate on water contact angle for $O_5$-DLC and $O_{40}$-DLC samples. The results showed that with increasing oxygen flow rate, the contact angle of O-DLC water decreased from 82.9±2.1° to 50±3°. The boundary between hydrophilicity and hydrophobicity is the contact angle of 65° [47]. The hydrophilicity of DLC films is sensitive to the $sp^2/sp^3$ bonding ratio on the surface [48]. Reports by others show that $sp^2$-rich surfaces exhibit higher contact angles than $sp^3$-rich surfaces [49, 50]. Reducing the contact angle of water is the result of increasing the surface energy. The incorporation of oxygen into the film structure led to an increase in surface energy and thus wettability. Surface energy consists of two important components, i.e., dispersion and polar components. The polar component represents surface interactions that are related to dipoles, while the diffuse component represents surface interactions that are based on temporal changes in the electron density. Π-bonding electrons of $sp^2$ carbon sites and dangling bonding electrons have a higher potential for polarization than σ-bonding electrons of $sp^3$ carbon sites. Therefore, the polar component of the surface energy of oxygen-doped films increases with increasing incorporation of oxygen into the film structure. Π-bonding electrons of $sp^2$ carbon sites and dangling bonding electrons have a higher potential for polarization than σ-bonding electrons of $sp^3$ carbon sites. Therefore, the polar component of the surface energy of oxygen-doped layers increases with the increase of oxygen incorporation into the film structure. Figure 5 shows the contact angle results of $N_5$- DLC and $N_{40}$- DLC films. With increasing nitrogen flow rate from 5 to 40, the contact angle of DLC thin films increased from 78° to 110°. Therefore, in our opinion, the enhancement of contact angle of DLC thin films upon increasing nitrogen flow rate may be attributed to the increase of $sp^2$ carbon clustering and ordering of $sp^2$ clusters and $sp^2$ content, as shown by Raman studies.

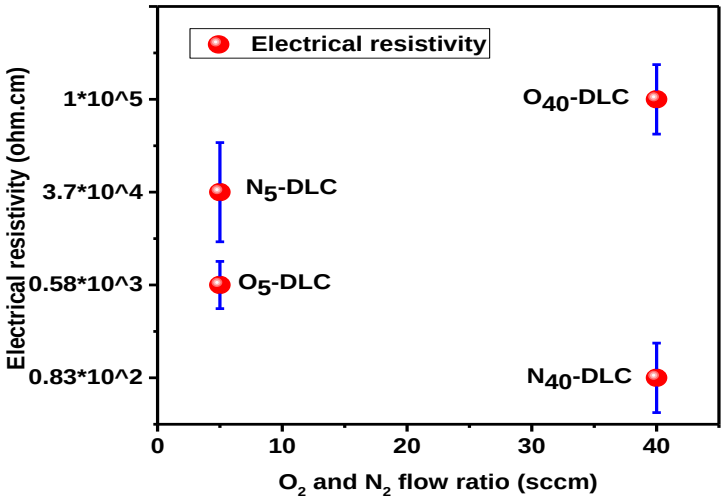


**Fig. 4.** The variation of electrical resistivity as a function of the oxygen flow rate.

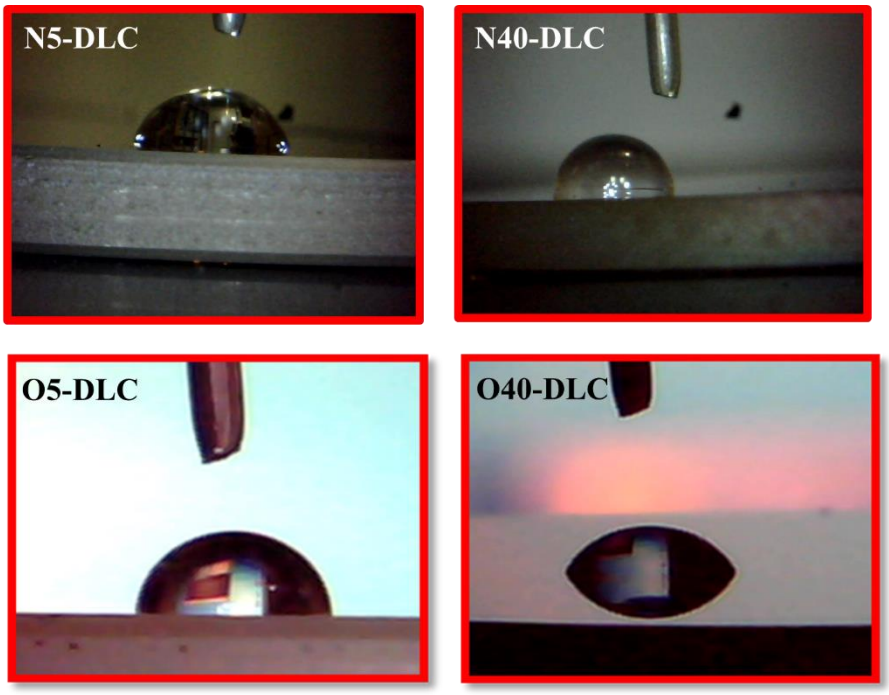


**Fig. 5.** The contact angle results of $O_5$- DLC, $O_{40}$- DLC, $N_5$- DLC and $N_{40}$- DLC films.

## 4. Conclusion

In this article, the comparison of electrical, structural, and hydrophobic properties of diamond-like carbon layers doped with oxygen and nitrogen was made. N-DLC and O-DLC samples were prepared using an anode layer system. The electrical resistivity of O-DLC films significantly reduced upon increasing the oxygen flow rate. By an increase in the oxygen content from 0 to 40 sccm, the internal stress decreased from 2.7 to 0.11 GPa. With increasing nitrogen flow rate (from 5 to 40 sccm) the internal stress of the deposited samples were decreased from 1.63 to 0.58 GPa. The water contact angle of O-DLC was found to decrease from 82.9°±2.1° to 50°±3° with the increase in oxygen flow rate. With increasing nitrogen flow rate from 5 to 40, the contact angle of DLC thin films increased from 78° to 110°. By doping nitrogen and oxygen, we showed that hydrophobic and hydrophilic layers can be produced by doping diamond-like carbon layer without any significant change in the morphology.

## References

[1] R. Zarei Moghadam, M. H. Ehsani, H. Rezagholipour Dizaji, P. Kameli and M. Jannesari, Modification of hydrophobicity properties of diamond like carbon films using glancing angle deposition method, Mater. Lett. 220 (2018) 301-304.

[2] M. K. Kuntumalla, V. V. S. S. Srikanth, S. Ravulapalli, U. Gangadharini, H. Ojha, N. R. Desai C. Bansal, SERS activity of Ag decorated nanodiamond and nano-β-SiC, diamond-like-carbon and thermally annealed diamond thin film surfaces, Chem. Phys. 17 (2015) 21331-21336.

[3] J. K. Luo, Y. Q. Fu, H. R. Le, J. A. Williams, S. M. Spearing, W. I. Milne, Diamond and diamond-like carbon MEMS, J. Micromech. Microeng. 17 (2007) 147-163.

[4] N. K. Aushik, P. Sharma, M. Nishijima, A. Makino, M. Esashi, S. Tanaka, Structural, mechanical and optical properties of thin films deposited from a graphitic carbon nitride target, Diamond. Relat. Mater. 66 (2016) 149-156.

[5] J. Robertson, Diamond-like amorphous carbon, Mater. Sci. Eng. R. 37 (2002) 129–281.

[6] P. Wang, T. Takeno, J. Fontaine, M. Aono, K. Adachi, H. Miki, T. Takagi, Effects of substrate bias voltage and target sputtering power on the structural and tribiological properties of carbon nitride coatings, Mater. Chem. Phys. 145 (2014) 434–440.

[7] K. Zhou, P. Ke, X. Li, Y. Zou, A. Wang, Microstructure and electrochemical properties of nitrogen-doped DLC films deposited by PECVD technique, Appl. Surf. Sci. 329 (2015) 281-286.

[8] M. Ikeyama, S. Nakao, Y. Miyagawa, S. Miyagawa, Effects of Si content in DLC films on their friction and wear properties, Surf. Coat. Technol. 191 (2005) 38–42.

[9] Sk. F. Ahmed, D. Banerjee, K. K. Chattopadhyay, The influence of fluorine doping on the optical properties of diamond-like carbon thin films, Vacuum. 84 (2010) 837-842.

[10] N. Nakamura, T. Itani, H. Chiba, K. Watanabe, K. Kurihara, Effects of $O_2$ Gas Addition on Diamond-Like Carbon Film Deposition MRS Online Proceedings Library Archive, (1999) 593.

[11] M. S. Hwang, C. Lee, Effects of oxygen and nitrogen addition on the optical properties of diamond-like carbon films, Mater. Sci. Eng. B. 75 (2000) 24-28.

[12] S. F. Durrant, S. G. Castro, J. I. Cisneros, N. C. da Cruz, M. A. Bica de Moraes, Amorphous oxygen-containing hydrogenated carbon films formed by plasma enhanced chemical vapor deposition, J. Vac. Sci. Technol. A. 14 (1996) 118-124.

[13] G. Adamopoulos, C. Godet, T. Zorba, K. M. Paraskevopoulos, D. Ballutaud, Electron cyclotron resonance deposition, structure, and properties of oxygen incorporated hydrogenated diamond like amorphous carbon films, J. Appl. Phys. 96 (2004) 5456-5461.

[14] Y. Wu, J. Chen, H. Li, L. Ji, Y. Ye, H. Zhou, Preparation and properties of Ag/DLC nanocomposite films fabricated by unbalanced magnetron sputtering, Appl. Surf. Sci. 284 (2013) 165–170.

[15] D. Bootkul, B. Supsermpol, N. Saenphinit, C. Aramwit, S. Intarasiri, Nitrogen doping for adhesion improvement of DLC film deposited on Si substrate by Filtered Cathodic Vacuum Arc (FCVA) technique, Appl. Surf. Sci. 310 (2014) 284-292.

[16] H. Li, M. Fang, Y. Hou, R. Tang, Y. Yang, C. Zhong, Q. Li, Z. Li, The different effect of the additional electron withdrawing cyano group in different conjugation bridge: the adjusted molecular energy levels and largely improved photovoltaic performance, ACS Appl. Mater. Interfaces. 8 (2016) 12134-12140.

[17] V. Kopustinskas, Š. Meškinis, V. Grigaliūnas, S. Tamulevičius, M. Pucėta, G. Niaura, R. Tomašiūnas, Ion beam synthesis of α-CNx: H films, Surf. Coat. Technol. 180 (2002) 151-152.

[18] M. Tsuchiya, K. Murakami, K. Magara, K. Nakamura, H. Ohashi, K. Tokuda, T. Takami, H. Ogasawara, Y. Enta, Y. Suzuki, and S. Ando, Structural and electrical properties and current–voltage characteristics of nitrogen-doped diamond-like carbon films on Si substrates by plasma-enhanced chemical vapor deposition, Jpn. J. Appl. Phys. 55 (2016) 065502.

[19] L. Cançado, A. Jorio, M. Pimenta, Measuring the absolute Raman cross section of nanographites as a function of laser energy and crystallite size, Phys. Rev. B. 76 (2007) 064304-064307.

[20] J. K. Shin, C. S. Lee, K. R. Lee, K. Y. Eun, Effect of residual stress on the Raman-spectrum analysis of tetrahedral amorphous carbon films, Appl. Phys. Lett. 78 (2001) 631-633.

[21] P. K. Chu, L. Li Characterization of amorphous and nanocrystalline carbon films, Mater. Chem. Phys. 96 (2006) 253-277.

[22] M. Kahn, M. Čekada, T. Schöberl, R. Berghauser, C. Mitterer, C. Bauer, W. Waldhauser, E. Brandstätter, Structural and mechanical properties of diamond-like carbon films deposited by an anode 6 layer source, Thin Solid Films. 517 (2009) 6502-6507.

[23] C. Casiraghi, A. Ferrari, J. Robertson, Raman spectroscopy of hydrogenated amorphous carbons, Phys. Rev. B. 72 (2005) 085401.

[24] G. Adamopoulos, C. Godet, T. Zorba, K. M. Paraskevopoulos, D. Ballutaud Electron cyclotron resonance deposition, structure, and properties of oxygen incorporated hydrogenated diamond like amorphous carbon films, J. Appl. Phys. 96 (2004) 5456–5461.

[25] N. Dwivedi, S. Kumar, H. K. Malik, Role of ex-situ oxygen plasma treatments on the mechanical and optical properties of diamond-like carbon thin films, Mater. Chem. Phys. 134 (2012) 7-12.

[26] T. McKindra, M. J. O'Keefe, R. Cortez, Reactive sputter-deposition of oxygenated amorphous carbon thin films in $Ar/O_2$, Diam. Relat. Mater. 20 (2011) 509-515.

[27] M. Chhowalla, A. Ferrari, J. Robertson, G. Amaratunga, Evolution of $sp^2$ bonding with deposition temperature in tetrahedral amorphous carbon studied by Raman spectroscopy, Appl. Phys. Lett. 76, (2000) 1419-1421.

[28] A. C. Ferrari and J. Robertson, Phys. Rev. B. 61, (2000) 14095.

[29] S. R. Polaki, K. Ganesan, S. K. Srivastava, M. Kamruddin, A. K. Tyagi, The role of substrate bias and nitrogen doping on the structural evolution and local elastic modulus of diamond-like carbon films, J. Phys. D. Appl. Phys. 50 (2017) 175601.

[30] M. K. Puchert, P. Y. Timbrell, R. N. Lamb, D. R. McKenzie, Thickness-dependent stress in sputtered carbon films, J. Vac. Sci. Technol. 12 (1994) 727-732.

[31] J. W. Zou, K. Reichelt, K. Schmidt, B. Dischler, The deposition and study of hard carbon films, J. Appl. Phys. 65 (1989) 3914-3918.

[32] R. Zarei Moghadam, M. H. Ehsani, H. Rezagholipour Dizaji, P. Kameli, and M. Jannesari, Oxygen doping effect on wettability of diamond-like carbon films, Mater. Res. Exp. 8 (2021) 035601.

[33] M. A. Tamor, W. C. Vassell, Raman "fingerprinting" of amorphous carbon films, J. Appl. Phys. 76 (1994) 3823-3830.
[34] M. A. Tamor, W. C. Vassell, K. R. Carduner, Atomic constraint in hydrogenated "diamond-like" carbon, Appl. Phys. Lett. 58 (1991) 592-594.
[35] J. Robertson, E. P. O'Reilly, Electronic and atomic structure of amorphous carbon, Phys. Rev. B. 35 (1987) 2946.
[36] S. R. P. Silva, J. Robertson, G. A. J. Amaratunga, B. Rafferty, L. M. Brown, J. Schwan, D. F. Franceschini, G. Mariotto. Nitrogen modification of hydrogenated amorphous carbon films, J. Appl. Phys. 81 (1997) 2626-2634.
[37] Y. B. Zhang, S. P. Lau, D. Sheeja, and B. K. Tay, Study of mechanical properties and stress of tetrahedral amorphous carbon films prepared by pulse biasing, Surf. Coat. Technol. 195 (2005) 338-343.
[38] Y. N. Kok, P. E. Hovsepian, Q. Luo, D. B. Lewis, J. G. Wen, I. Petrov, Influence of the bias voltage on the structure and the tribological performance of nanoscale multilayer C/Cr PVD coatings, Thin Solid Films 475 (2005) 219-226.
[39] T. Chen, X. Wu, Z. Ge, J. Ruan, B. Lv, and J. Zhang, Achieving low friction and wear under various humidity conditions by co-doping nitrogen and silicon into diamond-like carbon films, Thin Solid Films. 638 (2017) 375-382.
[40] D.-J. Jan, C.-F. Ai, C.-C. Lee, Deposition of nitrogen-containing diamond-like carbon films on acrylic substrates by an ion beam process, Vacuum. 74 (2004) 531-538.
[41] R. Zarei Moghadam, H. Rezagholipour Dizaji, M. H. Ehsani, Modification of optical and mechanical properties of nitrogen doped diamond-like carbon layers, J. Mater. Sci.: Mater. 30 (2019) 1-12.
[42] E. Mohagheghpour, M. Rajabi, R. Gholamipour, M. M. Larijani, S. Sheibani, Correlation study of structural, optical and electrical properties of amorphous carbon thin films prepared by ion beam sputtering deposition technique, Appl. Surf. Sci. 360 (2016) 52-58.
[43] C. Chung, S. Chen, P. Chiu, M. Chang, T. Hung, T. Ko, Carbon film-coated 304 stainless steel as PEMFC bipolar plate, J. Power Sources. 176 (2008) 276–281.
[44] M. Chhowalla, A. C. Ferrari, J. Robertson, G. A. J. Amaratunga, Evolution of $sp^2$ bonding with deposition temperature in tetrahedral amorphous carbon studied by Raman spectroscopy, Appl. Phys. Lett. 76 (2000) 1419–1421.
[45] R. Zarei Moghadam, H. Rezagholipour Dizaji, M. H. Ehsani, P. Kameli, and M. Jannesari. Correlation study of structural, optical, and hydrophobicity properties of diamond-like carbon films prepared by an anode layer source. Mater Res Exp 6 (2019) 055601.
[46] T.F. Zhang, K.W. Kim, K.H. Kim, Nitrogen-incorporated hydrogenated amorphous carbon film electrodes on Ti substrates by hybrid deposition technique and annealing, J. Electrochem. Soc. 163 (2016) 54–61.
[47] E. A. Vogler Structure and reactivity of water at biomaterial surfaces, Adv. Colloid Interface. 74 (1998) 69–117.
[48] L. Y. Ostrovskaya, Studies of diamond and diamond-like film surfaces using XAES, AFM and wetting Vacuum. 68 (2002) 219–238.
[49] E. Gribanova, A. Zhukov, I. Antonyuk, C. Benndorf, E. Baskova, Effect of the acidity of aqueous solutions on the wettability of diamond, graphite and pyrocarbon surfaces, Diamond Relat. Mater. 9 (2000) 1–6.
[50] F. Piazza, G. Morell Wettability of hydrogenated tetrahedral amorphous carbon, Diamond Relat. Mater. 18 (2009) 43–50.